

Scaling laws for partially developed turbulence

Abigail Hsu^{1†}, Ryan Kaufman^{1‡}, and James Glimm^{1¶}

¹Stony Brook University, Stony Brook NY 11794

We formulate multifractal models for velocity differences and gradients which describe the full range of length scales in turbulent flow, namely: laminar, dissipation, inertial, and stirring ranges. The models subsume existing models of inertial range turbulence. In the localized ranges of length scales in which the turbulence is only partially developed, we propose multifractal scaling laws with scaling exponents modified from their inertial range values. In local regions, even within a fully developed turbulent flow, the turbulence is not isotropic nor scale invariant due to the influence of larger turbulent structures (or their absence). For this reason, turbulence that is not fully developed is an important issue which inertial range study can not address. In the ranges of partially developed turbulence, the flow can be far from universal, so that standard inertial range turbulence scaling models become inapplicable. The model proposed here serves as a replacement. Details of the fitting of the parameters for the τ_p and ζ_p models in the dissipation range are discussed. Some of the behavior of ζ_p for larger p is unexplained. The theories are verified by comparing to high resolution simulation data.

Key words: turbulence, multifractals, scaling law, structure functions, intermittency

1. Introduction

We develop a conceptual framework for turbulent scaling laws across length scales extending beyond the inertial range. Classically, fully developed turbulence is defined as occurring on length scales in which energy transfer is dominated by inertial forces. Partially developed turbulence is defined as turbulent (i.e. non-laminar) ranges in which turbulence may or may not be fully developed. Thus, length scales with significant dissipation and stirring forces are included within partially developed turbulence. We propose new models with supporting verification which subsume and extend inertial and non-inertial range models of others. From our models and data analysis, we explain phenomena not previously observed and phenomena previously observed but not explained.

The inertial range is defined as an intermediate range of length scales, l , which are far from the Kolmogorov scale η and integral scale L , i.e. $\eta \ll l \ll L$. The dissipation range is the range of length scales between the laminar range and the inertial range. The stirring range, in many observational, experimental and simulation studies, is the range of length scales larger than the inertial range.

Structure functions give a precise meaning to clustering of bursts of turbulent intensity

† Email address for correspondence: abigail.hsu2009@gmail.com

‡ Email address for correspondence: rykauf@gmail.com

¶ Email address for correspondence: glimm@ams.sunysb.edu

and compound clustering (i.e. clustering of clusters) etc. They measure the dependence of these compound clustering rates on the length scale set by the observational size of the cluster. Two families of structure functions are studied here: one characterizes the powers of the energy dissipation rate, ϵ , and the other characterizes powers of the velocity difference, δu .

The total turbulent energy dissipation rate ϵ in homogeneous turbulence is defined as the global spatial integral of:

$$\epsilon(\vec{x}, t) = \frac{\nu}{2} \left(\frac{\partial u_i}{\partial x_j} + \frac{\partial u_j}{\partial x_i} \right)^2, \quad (1.1)$$

where ν is the kinematic viscosity of the fluid and the summation convention is implied. We define the coarse grained, local average of the dissipation rate ϵ_l as,

$$\epsilon_l(\vec{x}) = \frac{1}{|V_l|} \iiint_{V_l(\vec{x})} \epsilon(\vec{y}, t) d\vec{y}, \quad (1.2)$$

where $V_l(\vec{x})$ is a volume with a diameter l centered around \vec{x} in 3D. The coarse grained averaging means that ϵ_l reflects properties occurring on the length scale l .

The structure functions of $\delta_l u$ and ϵ_l satisfy asymptotic scaling relations as a power of the length scale l . The structure functions and the associated scaling exponents τ_p and ζ_p are given by the expectation relations,

$$\langle (\epsilon_l)^p \rangle \sim l^{\tau_p} \quad \text{and} \quad \langle |\delta_l u|^p \rangle \sim l^{\zeta_p}. \quad (1.3)$$

The length scale dependent scaling exponents τ_p and ζ_p are obtained from logarithmic local slopes, i.e.

$$\tau_p = \frac{d(\ln \langle \epsilon_l^p \rangle)}{d(\ln l)} \quad \text{and} \quad \zeta_p = \frac{d(\ln \langle |\delta_l u|^p \rangle)}{d(\ln l)}, \quad (1.4)$$

as suggested by L. Miller & E. Dimotakis (1991).

The main thrust of the theory is that turbulent scaling laws remain in effect across all length scale ranges, but with modified length dependent scaling exponents.

A key step in the parameterization of the introduced scaling models is that τ_p and ζ_p in eq. (1.4) are linear in $\ln l$ in the dissipation range. Hence, the slopes of τ_p and ζ_p are constructed,

$$T_p = \frac{d(\tau_p)}{d(\ln l)} \quad \text{and} \quad Z_p = \frac{d(\zeta_p)}{d(\ln l)}, \quad (1.5)$$

which are modeled across all length scales as piecewise constant.

The piecewise constant values of T_p and Z_p appear to be a new discovery. These piecewise constant values over the 4 length scale ranges are described as follows:

$$T_p = \begin{cases} 0, & \text{laminar range (LR)} \\ T_p^{dr}, & \text{dissipation range (DR)} \\ 0, & \text{inertial range (IR)} \\ T_p^{sr}, & \text{stirring range (SR)} \end{cases} \quad Z_p = \begin{cases} 0, & \text{laminar range (LR)} \\ Z_p^{dr}, & \text{dissipation range (DR)} \\ 0, & \text{inertial range (IR)} \\ Z_p^{sr}, & \text{stirring range (SR)} \end{cases} \quad (1.6)$$

In the inertial range, we take $T_p = 0$. We do not observe $T_p = 0$ from our data in this range, but include this to be consistent with the classical model by She & Leveque (1994), denoted SL, in lieu of a more comprehensive theory.

T_p^{dr} and Z_p^{dr} are constant in the dissipation range, and T_p^{sr} and Z_p^{sr} are constant in the stirring range for the problems we study. These T_p and Z_p values are verified in the

JHTDB and the T_p values in the UMA data. In addition, we observe that T_p is linear in p , and Z_p is given by an explicit p dependent formula in the dissipation range.

In the dissipation range, the logarithmic dissipation rate is proportional to $\ln(l)$. In contrast, the dissipation defined in the Navier-Stokes equation itself occurs in the laminar range at a rate proportional to the length scale l . For $p = 2$, the laminar energy dissipation rate ϵ includes the classical viscosity ν within its definition. The increase of both τ_p and ζ_p for all p in a limit as l approaches η from above leads to negative constant values of T_p and Z_p in their respective dissipation ranges.

The key property of constant slopes T_p and Z_p is also satisfied in the stirring range and observed in the JHTDB data. In principle, stirring forces can be added in an arbitrary manner at any length scale. Parameterization of the stirring range is not addressed in this paper.

We provide a brief literature review in Sec. 2. The numerical verification data from JHTDB and UMA are described in Sec. 3 as well as the methods used for data analysis. The scaling law results, which are the technical core of the paper, are presented in Secs. 4 and 6. The extended and refined scaling analytical methods are discussed in Sec. 5. A comment on the asymptotics of the viscous limit can be found in Sec. 7. Conclusions are summarized in Sec. 8.

2. Inertial range prior results

Kolmogorov (1941), denoted K41, postulated universal laws to govern the statistics on all such length scales in the inertial range in which the flow is statistically self similar. Dimensional analysis in K41, based on the self similarity hypothesis, led to the $-5/3$ scaling law. However, because the energy dissipation for turbulent flows is intermittent, this model has been refined in various ways over the years to yield a multifractal scaling law. Summarized in Frisch (1996), the K41 exponent ζ_p is modified to capture the compound clustering of turbulent structure using a multifractal analysis. Kolmogorov (1962) refined his similarity hypothesis, denoted K62, added the influence of the large flow structure and included the influence of the intermittency. The refined similarity hypothesis in Kolmogorov (1962) for the classical inertial range links the scaling exponent ζ_p of the longitudinal velocity structure and the scaling exponent τ_p of the energy dissipation rate as

$$\langle |\delta_l u|^p \rangle \sim \langle \epsilon_l^{p/3} \rangle l^{p/3}, \quad (2.1)$$

where $\langle \epsilon_l^{p/3} \rangle \sim l^{\tau_{p/3}}$, or equivalently

$$\zeta_p = \frac{p}{3} + \tau_{\frac{p}{3}}. \quad (2.2)$$

The log-normal model from SL defines a theoretical model for the PDF of the coarse-grained energy dissipation in the inertial range. SL studied the quantity $\epsilon_l^{(p)}$ defined as the ratio:

$$\epsilon_l^{(p)} = \frac{\langle \epsilon_l^{p+1} \rangle}{\langle \epsilon_l^p \rangle}. \quad (2.3)$$

where p can be any non-negative integer. The $\epsilon_l^{(0)}$ and $\epsilon_l^{(\infty)}$ are related to the mean fluctuation structure $\bar{\epsilon}$ and the filamentary structure. The scaling law for $p \rightarrow \infty$ is $\epsilon_l^{(\infty)} \sim l^{-2/3}$. As $p \rightarrow \infty$, the definition of τ_p stating that,

$$\tau_{p+1} - \tau_p \longrightarrow -\frac{2}{3}, \quad (2.4)$$

or $\tau_p = -\frac{2}{3} \cdot p + C$. The codimension C is evaluated as $C = 3 - 1 = 2$ based on the assumption that the elementary filamentary structures have dimension 1. The expectation $\langle \epsilon_l^p \rangle$ has an l dependence which is not a pure exponential, but a mixture of exponentials, i.e. the scaling exponents for $\langle \epsilon_l^p \rangle$ are defined as a weighted average of exponentials.

From the assumption of the interaction between structures of different order, SL proposed the following relation between structures of adjacent order:

$$\epsilon_l^{(p+1)} = A_p \epsilon_l^{(p)\beta} \epsilon_l^{(\infty)^{1-\beta}}. \quad (2.5)$$

Based on eqs. (2.3, 2.5), SL derives a two step recursion for τ_p . This recursion relation implies that $\tau_p = -\frac{2}{3} \cdot p + 2 + f(p)$, where $f(\infty) = 0$ is assumed. The equation for $f(p)$ has the solution $f(p) = \alpha \beta^p$ and with the boundary conditions $\tau_0 = \tau_1 = 0$, the solution becomes

$$\tau^{SL}(p) = -\frac{2}{3} \cdot p + 2 \left[1 - \left(\frac{2}{3} \right)^p \right]. \quad (2.6)$$

Substituting eq. (2.6) into the relation shown in (2.2) yields

$$\zeta_p = \frac{p}{9} + 2 \left[1 - \left(\frac{2}{3} \right)^{\frac{p}{3}} \right]. \quad (2.7)$$

Novikov (1994) suggested that the $-2/3$ on the RHS of eq. (2.4) should be replaced by -1 based on the theory of infinitely divisible distributions applied to the scaling of the locally averaged energy dissipation rate ϵ_l . Chen & Cao (1995), denoted CC, accepted Novikov's suggestions and derived the formula:

$$\tau^{CC}(p) = -p + [(1 + \tau_2)^p - 1]/\tau_2, \quad (2.8)$$

which uses the classical value $\tau_2 \approx -0.22$, which is derived from simulations, observations, experiments, and theory (SL) all in approximate agreement.

Kolmogorov proposed that $\zeta_3 = 1$ for incompressible, isotropic and homogeneous turbulence. Frick *et al.* (1995) showed that in the case of nonhomogeneous shell models with $\zeta_3 \neq 1$, the scaling of velocity structure functions in incompressible turbulence from SL still holds as $\zeta_p/\zeta_3 = p/9 + 2[1 - (2/3)^{\frac{p}{3}}]$.

Boldyrev *et al.* (2002) predicted a new scaling law for the scaling exponent ζ_p of velocity structure functions as

$$\zeta_p/\zeta_3 = p/9 + 1 - (1/3)^{\frac{p}{3}}, \quad (2.9)$$

in supersonic turbulence for star formation based on a Kolmogorov-Burgers model. The same behavior is observed by Müller & Biskamp (2000) in incompressible MHD.

The SL model has generated a considerable interest in the hierarchical nature of turbulence. Experiments and simulations have been conducted to evaluate the velocity and energy dissipation structures. Chavarria *et al.* (1995a,b, 1996) demonstrated experimental variables for the hierarchical structure assumption for the function ζ_p in eq. (2.7). Experimental studies on a turbulent pipe flow and a turbulent mixing layer by Zou *et al.* (2003) verified the SL hierarchical symmetry. Cao *et al.* (1996) showed agreement between the SL scaling exponents and high-resolution direct numerical simulations (DNS) of 3D Navier-Stokes turbulence. Further references are added as needed through out the paper.

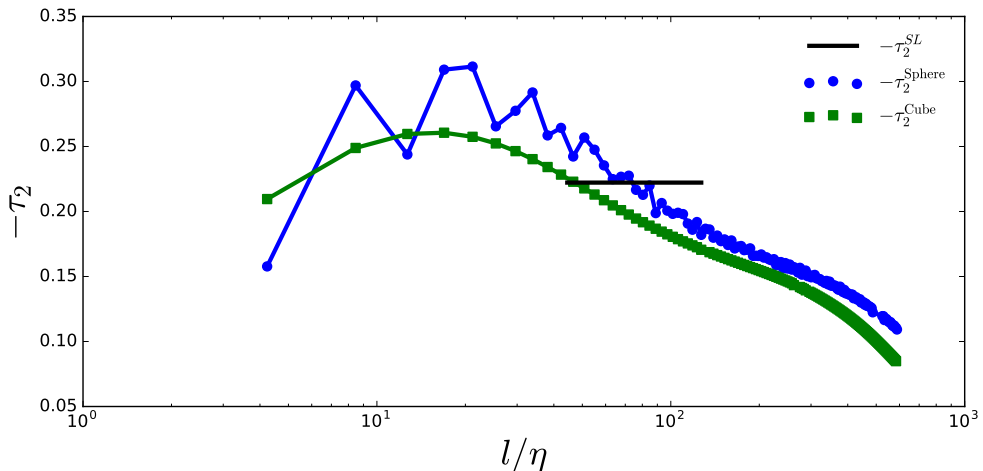


Figure 1: Comparison of the cubic to the spherical average with a diameter l for ϵ_l in the computation of $-\tau_2$. The horizontal solid line is the constant local exponent $-\tau_2^{SL}$ value from SL and is located at the inertial range that is determined by ζ_2 from JHTDB.

3. Methods

3.1. JHTDB data

We analyze the DNS data of the forced isotropic turbulence simulation from the Johns Hopkins Turbulence Database (JHTDB) performed by Li *et al.* (2008) and Perlman *et al.* (2007). The simulated flow has an integral scale Reynolds number $Re = 23,298$ and a Taylor scale Reynolds number $Re_\lambda = 433$. The JHTDB data are generated by direct numerical simulation of forced isotropic turbulence in a cubic domain with length $L = 2\pi$ and periodic boundary conditions in each direction. The simulation has a resolution of 1024^3 of cells. Energy is injected to maintain a constant value for the total energy. The JHTDB data are collected after the simulation has reached a statistical stationary state. The data are posted on the website <http://turbulence.pha.jhu.edu>

The JHTDB data focus on analysis of the inertial range. Because of this emphasis, its coverage of the dissipation and stirring ranges is limited. The ratio of the Kolmogorov length scale to the computational grid space is $\eta/\Delta x = 0.46$. Thus, the JHTDB data do not fully resolve the Kolmogorov length scale η . With these data, we confirm many aspects of our scaling law model. We anticipate the need for additional simulation data such as the 4096^3 cell data from the JHTDB in further analysis of laminar and dissipation ranges.

3.2. JHTDB data analysis

The velocity differences have a tensorial dependence on the velocity component directions and the differencing directions. The longitudinal direction is more convenient for experiments, and many experimental prior studies focused on the longitudinal velocity increment based on Taylor's hypothesis. Details are described by He *et al.* (1999). We define the longitudinal velocity increment as $\delta_l u(x, y, z, t) = u(x + l, y, z, t) - u(x, y, z, t)$, where u is the x component of velocity.

The coarse-graining length scale, l , in the structure function definition, eq. (1.2) is

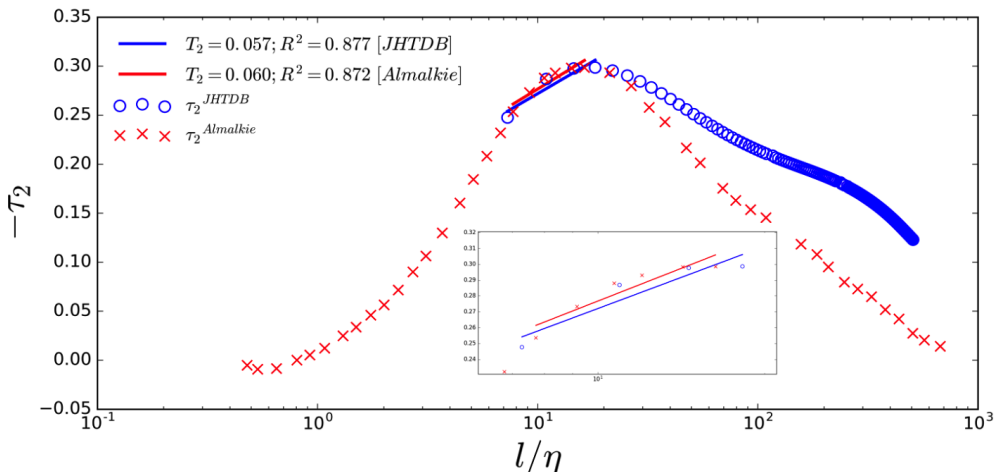


Figure 2: Consistency of the JHTDB and UMA data. The inset is a refined image of the overlapped dissipative ranges.

implemented by a 3D average over distances of a scale l , and ϵ is given at discrete locations in space. From previous literature, the averaging volume is taken to be a sphere or a cube. The definition of l as radius or diameter is not consistent in the literature. In this paper, we distinguish between spherical and cubic average with a diameter l . The dominant effects on the averaging element, sphere or cube, come from the most extreme points on the elements, i.e. the boundary of the sphere or corners of the cube, and always with these extreme points at distance $l/2$ from the center.

In Fig. 1, we observe an approximate but not exact agreement between the cubic and spherical averages. The cubic average, producing a consistent but less noisy range, is used for the local average of the energy dissipation rate in this paper.

A further observation is that τ_2 in the inertial range is not consistent with prevailing theory i.e. τ_2 is not constant while ζ_2 is constant in this range. Fig. 1 shows the theoretical value for the inertial range τ_2^{SL} as a horizontal line. The local slope measurements are points connected by line segments. While an average across a large range is consistent with SL, no universal constant local slope is found that is consistent with τ_2^{SL} . For this reason, we regard the τ_p theory from SL more exactly as a theory for ζ_p rather than a theory for τ_p .

3.3. UMA data analysis

The UMA data from Almalkie & De Bruyn Kops (2012) are based on a DNS of isotropic homogeneous turbulence from the University of Massachusetts Amherst (UMA). This simulation uses a third-order Adams-Bashforth and pseudo-spectral method. The simulation uses a periodic cube with edge length 2π and a 2048^3 numerical grid. The simulation parameters are $\eta/\Delta x = 3.04$ and $\eta k_{max} = 6.4$. The flow has an integral scale Reynolds number $Re = 3,426$ and a Taylor scale Reynolds number $Re_\lambda = 151$. The inertial range turbulence is fully developed and the data also describe with a complete dissipation range with length scales smaller than the Kolmogorov length scale. There are sufficient data to provide verification in the laminar range. We digitized the local slopes $-\tau_p$ from the published UMA data for $p = 2, 3, 4$ by Almalkie & De Bruyn Kops (2012).

The UMA locally averaged dissipation rate ϵ_l data are defined as a spherical average

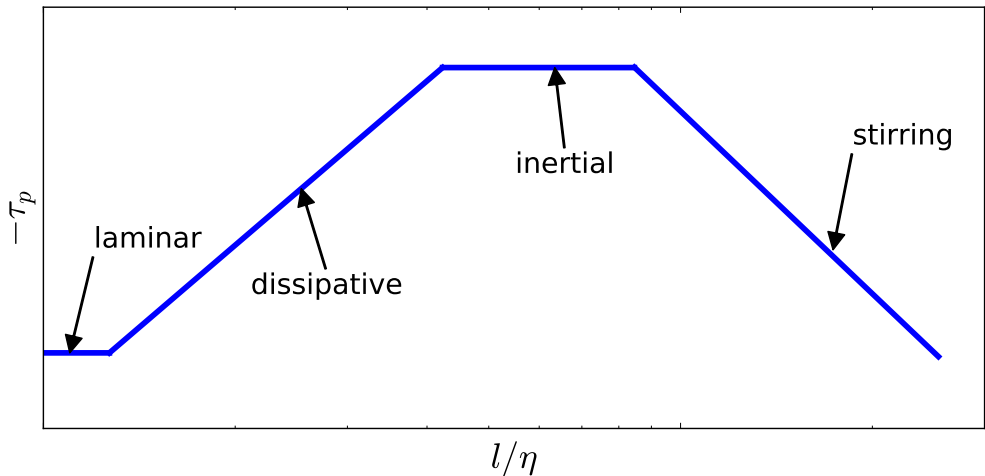


Figure 3: Schematic representation of $-\tau_p$ vs. l/η on a semi-log scale.

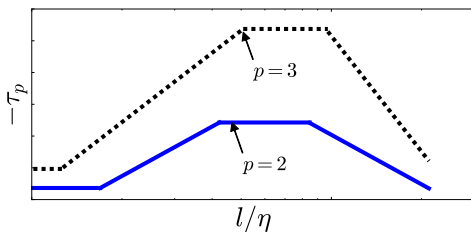


Figure 4: Schematic representation of the local slope, $-\tau_p$ vs. log length scale with the p -dependence shown by the arrow.

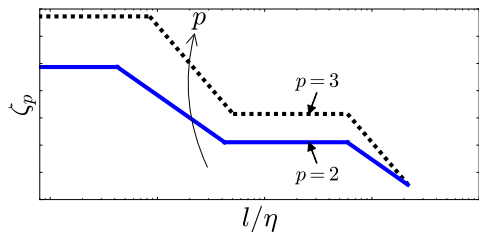


Figure 5: Schematic representation of the local slope, ζ_p vs. log length scale with the p -dependence shown by the arrow.

with a diameter l . An interpolation consistent with the numerical method is used to solve the governing equations and allows the elimination of the noise.

As noted in Fig. 1, the spherical average leads to a higher $-\tau_p$ value than the cubic average. A vertical shift of 0.04 for $-\tau_2$ of the cubic averaged JHTDB data is needed to reach the spherical averaged UMA maximum for comparison. In addition, a horizontal shift of the normalized length scale l/η is needed to compensate for the JHTDB under resolution of the Kolmogorov scale. In Fig. 2, we see that the linear local slope is clearly defined in the dissipation range from the UMA $-\tau_2$ data and extends the JHTDB data. A refined inset shows the overlap from the two datasets after these shifts.

3.4. Schematic model formulation

Fig. 3 summarizes our major ideas. The laminar, dissipation, inertial and stirring ranges are labeled. This figure displays the slopes, T_p , as linear segments in the dissipation and stirring ranges. In Figs. 1 and 2, $-\tau_2$ does not show a clear flat range to indicate the classical inertial range. The flat segment shown in the schematic representation is taken from the SL theory. We comment on its absence from the JHTDB and UMA data in Sec. 4.3.

Figs. 4 and 5 show that as p increases, so do the values for $-\tau_p$ and ζ_p . Laminar flow

occurs at a nearly zero and is shown as a nearly horizontal line on the semi-log plots in Figs. 3, 4 and 5. The linearity of τ_p in the dissipation range implies the equation

$$\tau_p = T_p \ln \left(\frac{l}{\eta} \right) + b_p, \quad (3.1)$$

where T_p represents the constant slope observed in τ_p and b_p is the τ_p value at the Kolmogorov length scale (η).

Similarly, in the dissipation range, we define

$$\zeta_p = Z_p \cdot \ln \left(\frac{l}{\eta} \right) + a_p, \quad (3.2)$$

where Z_p represents the constant slope observed in ζ_p and $a_p = \zeta_p$ at the Kolmogorov length scale (η).

A transition point in the schematic representation occurs at the length scale where the slope of τ_p or ζ_p changes. The transition from turbulent dissipation to laminar dissipation occurs approximately at $l = \eta$. The detailed locations of the transition are dependent on p and are different for ζ_p and τ_p . The transition actually occurs gradually rather than discontinuously as we see in Fig. 6. However, in our modeling, T_p and Z_p are piecewise constant in $\ln l$ as an approximation to an exact theory. All other transitions are determined similarly.

In this modeling, ζ_p or τ_p for each p defines its own inertial range. The SL model holds within the inertial range defined by ζ_p .

4. Scaling laws for the energy dissipation rate

4.1. The laminar range

The digitized UMA data of $-\tau_p$ for $p = 2, 3, 4$ in the laminar range is shown in Fig. 6. $-\tau_2$ and $-\tau_3$ are close to zero here with, perhaps, a small p dependence shown in the τ_4 data. Thus, we assume that the τ_p values are approximately zero in the laminar range in which $l/\eta < 1$.

4.2. The p -dependent linear slopes in the dissipation range

The UMA data of Fig. 7 and the JHTDB of Fig. 8 show the linear segment of τ_p in the dissipation range. With limited data in small length scales but including higher p values (up to $p = 10$), we reach the same conclusion from Fig. 9 for the JHTDB data. The solid lines are modeled by the CC_2 model and will be explained in Sec. 5. The linear slopes are determined by least squares.

Recall that $\tau_p = T_p \ln(l/\eta) + b_p$. In Fig. 10, we plot the T_p for p up to 30 in the dissipation range. The slopes, T_p , are linear in p , with a T_2 data dependence, i.e.

$$T_p = \frac{dT_p}{dp} \cdot p + (T_2 - 2 \cdot \frac{dT_p}{dp}). \quad (4.1)$$

We find that $dT_p/dp = -0.323$ from the JHTDB data.

4.3. Full τ_p parameterization

We have developed a model that captures all of the length scales from the laminar range up to the small length scale end of inertial range for the energy dissipation rate. Based on eq. (4.1) and the assumption of $\tau_p \approx 0$ in the laminar range. A model for τ_p in

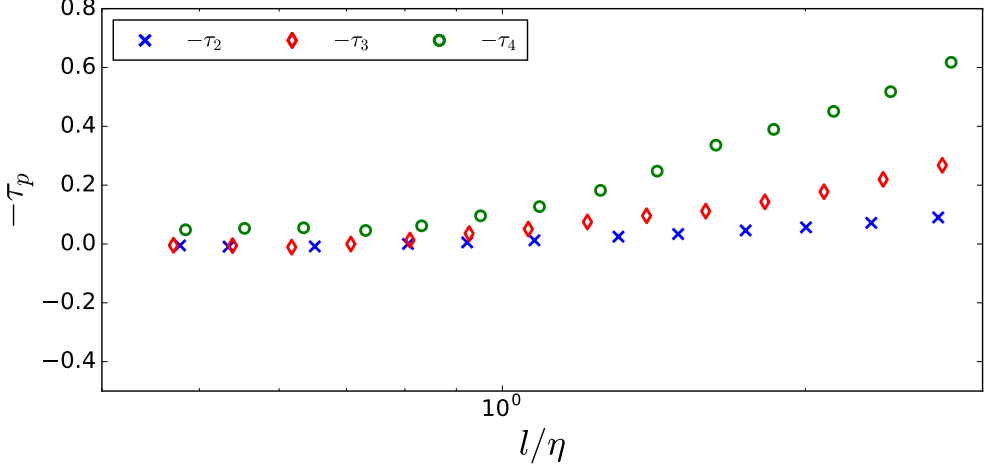


Figure 6: The digitized $-\tau_p$ values from the UMA data enlarged for the laminar range, for $p = 2, 3, 4$. We observe constant $-\tau_p$ values with weak p dependence for smaller lengths.

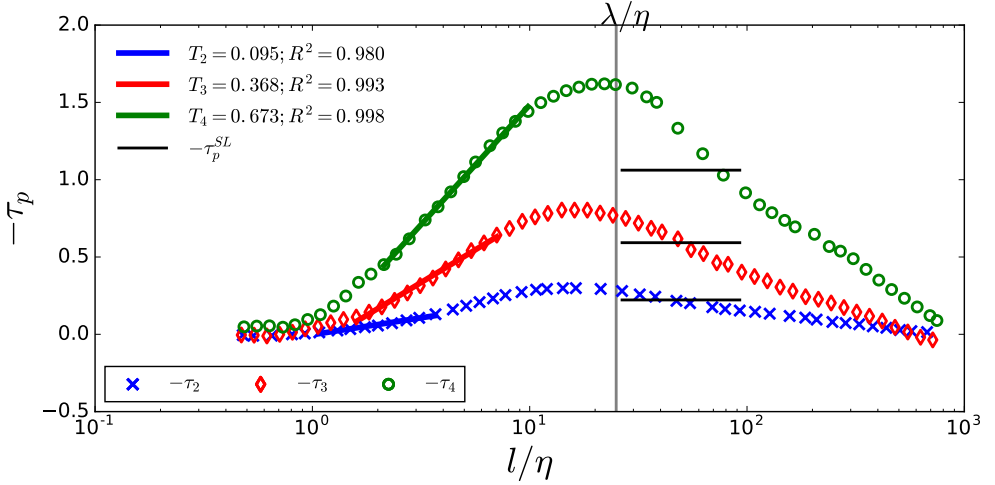


Figure 7: The digitized $-\tau_p$ UMA data. The horizontal solid lines are the constant local exponent $-\tau_p$ values from SL with the inertial range determined by ζ_2 from JHTDB. The vertical line marks the Taylor micro scale.

the dissipation range is

$$\tau_p^{dr} = \left(\frac{dT_p}{dp} \cdot p + \left(T_2 - 2 \cdot \frac{dT_p}{dp} \right) \right) \cdot \ln \left(\frac{l}{\eta} \right), \quad (4.2)$$

which can be extended for length l up to the Taylor micro-scale λ .

In the JHTDB and UMA data, there is no flat inertial range observed for τ_p and the τ_p peak occurs approximately at the Taylor micro-scale λ . The peak could be an isolated point represents a transition to the stirring range. Alternatively, there maybe a small

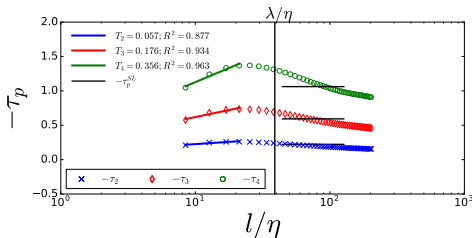


Figure 8: The local slopes $-\tau_2, -\tau_3, -\tau_4$ from the JHTDB data are linear in $\ln(l/\eta)$ in the dissipative ranges, with constant slopes T_p . An R^2 value closes to 1 indicates the goodness of the fit.

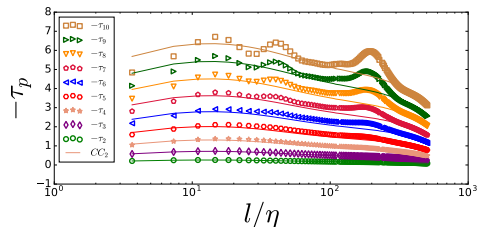


Figure 9: The local slope τ_p for all $2 \leq p \leq 10$ with p increasing from the bottom to the top. The JHTDB data are shown in scatter points and the modeled $-\tau_p$ values are in solid lines from the CC_2 model explained in Sec. 5.

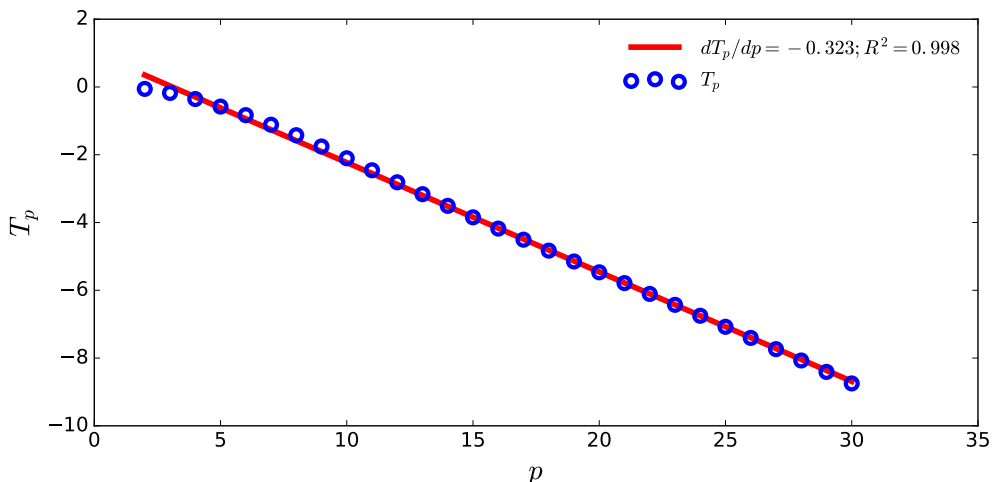


Figure 10: The T_p in the dissipative range is linear for p in the range $2 \leq p \leq 30$ for the JHTDB data.

inertial range and a large transition range, in which case, it is possible that with higher Reynolds number, a true (flat) inertial range for τ_p may appear.

5. The extended and refined CC models for the scaling exponent of the energy dissipation rate

The CC model defined by Chen & Cao (1995) shown in eq. (2.8) has a dependence on inertial constant $\tau_2 = \tau_2^{SL} \approx -0.22$ value from SL. We extend the model beyond the inertial range, where a constant τ_2^{SL} is no longer an accurate value for length scale dependent τ_2 . To calculate τ_p for $p > 2$, we substitute the τ_2 data that are measured across all length scales into eq. (2.8). The extended model is denoted as the CC_2 model. Fig. 11 shows this model for τ_3 (solid line) in comparison to the observed τ_3 value (data points). The same comparison for $p \leq 10$ is shown in Fig. 9. The data and model values

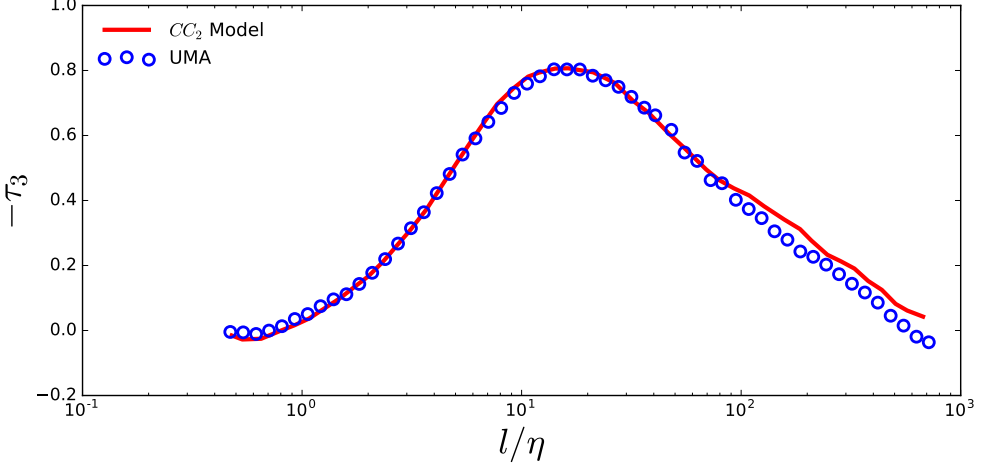


Figure 11: The extended CC_2 model for $-\tau_3$ shows agreement with the UMA data across all measurable length scales.

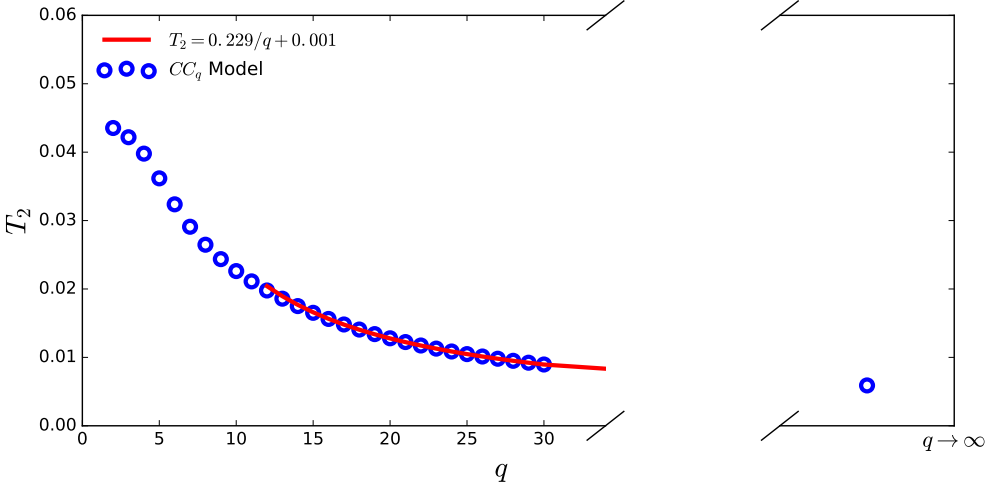


Figure 12: The linear slopes T_2 of τ_2 calculated from the CC_q model for q from 2 to 30 using JHTDB is plotted vs. q in the dissipative range.

agree for small $p \leq 5$, but diverge at higher p values. We propose a modification of CC_2 , which we denote as CC_q model. Instead of taking a measured τ_2 , as in our extended CC_2 model, we substitute the measured τ_q data that is available across all measurable length scales, and solve numerically for $\hat{\tau}_2$ shown as below:

$$\tau_q = -q + [(1 + \hat{\tau}_2)^q - 1]/\hat{\tau}_2. \quad (5.1)$$

Then, the calculated $\hat{\tau}_2$ can be substituted back to eq. (2.8) to calculate τ_p for any p . From this point, all τ_p values can be modeled as a function of p and the measured τ_q using the CC_q model.

Fig. 12 shows the linear fit T_2 of τ_2 that is calculated from the CC_q model using

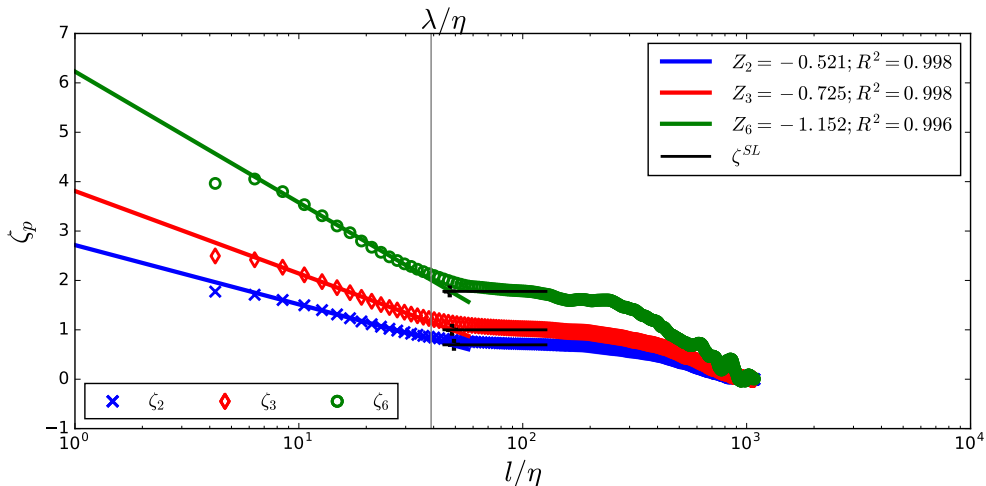


Figure 13: $\zeta_2, \zeta_3, \zeta_6$ are linear in the dissipative ranges with the solid line representing the linear fit of ζ_p in the dissipation range, extrapolated to the Kolmogorov scale for the JHTDB data. The horizontal lines are the corresponding SL model values and the vertical line marks the Taylor micro-scale. The bold ‘+’ near the Taylor scale values λ/η are the transition points from the dissipation ranges to the inertial ranges.

measured τ_q values in the dissipation range, for $q = 2, 3, \dots, \infty$. This sequence of T_2 values are fitted by:

$$T_2 = 0.229/q + 0.001 \quad (5.2)$$

for any q value. T_2 decreases and converges asymptotically to 0.001 as $q \rightarrow \infty$. Hence, the CC_∞ model is defined as $CC_\infty = \lim_{q \rightarrow \infty} CC_q$.

6. Scaling laws for the longitudinal velocity increment structure functions

6.1. The p -dependent linear slopes in the dissipation range

The JHTDB data for the slopes Z_p of the longitudinal velocity increment $\langle |\delta_l u_1|^p \rangle$ vs. $\ln(l/\eta)$ for $p = 2, 3, 6$ are shown in Fig. 13. We see that ζ_p is consistent with the horizontal solid lines of ζ_p^{SL} values obtained from eq. (2.7) in the inertial range. In addition, ζ_p is linear in $\ln(l/\eta)$ in the dissipation range. Summary data for all p up to 10 are given in Fig. 14 with linear extrapolation from the dissipation range to the Kolmogorov scale for the JHTDB data.

Recall that $\zeta_p = Z_p \ln\left(\frac{l}{\eta}\right) + a_p$ in our linear model for longitudinal velocity increment in the dissipation range. This equation gives a new relation for the linear slope ratio Z_p/Z_3 and the ratio a_p/a_3 as:

$$\begin{aligned} \zeta_p/\zeta_3 &= \frac{Z_p \cdot \ln\left(\frac{l}{\eta}\right) + a_p}{Z_3 \cdot \ln\left(\frac{l}{\eta}\right) + a_3} \\ &= \frac{Z_p + a_p/\ln\left(\frac{l}{\eta}\right)}{Z_3 + a_3/\ln\left(\frac{l}{\eta}\right)}. \end{aligned} \quad (6.1)$$

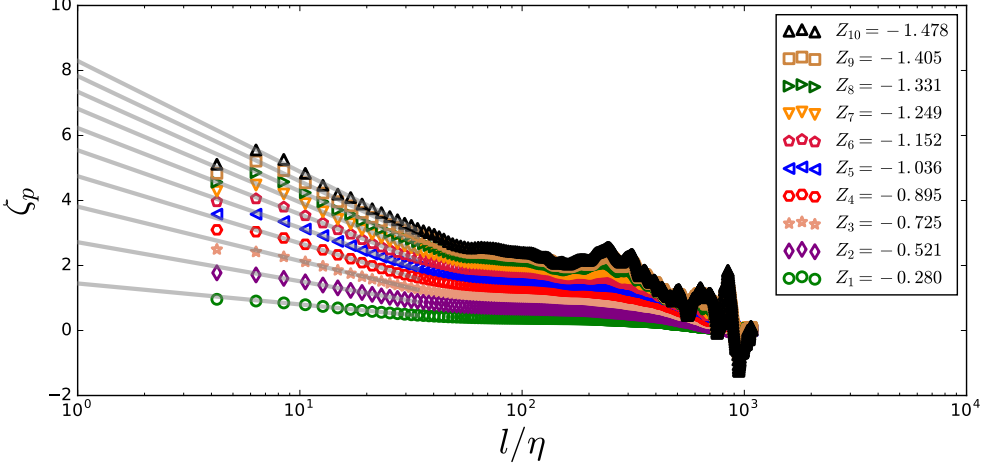


Figure 14: The JHTDB defined ζ_p with p increasing from 1 to 10 from the bottom to the top across all available length scales. The plot shows scatter points with solid lines representing the linear fit of ζ_p in the dissipation range extrapolated to the Kolmogorov scale.

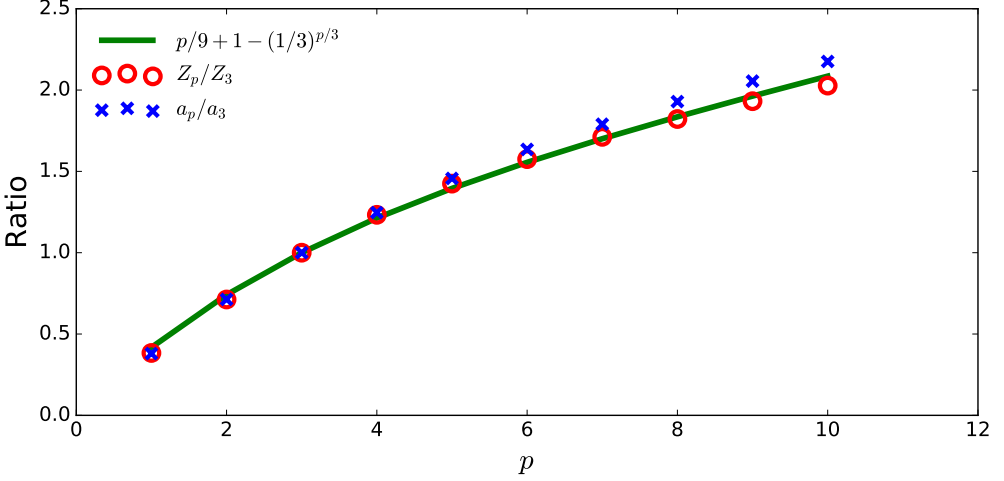


Figure 15: The new ratio model agrees with the ratios of Z_p/Z_3 and of a_p/a_3 from JHTDB data in the dissipation range.

Based on the model representation (2.9) and on eq. (6.1), we develop a model for the longitudinal velocity structure in the dissipation range as:

$$\begin{aligned} Z_p/Z_3 &= p/9 + 1 - (1/3)^{p/3}, \\ a_p/a_3 &= p/9 + 1 - (1/3)^{p/3}. \end{aligned} \quad (6.2)$$

This law is valid for the JHTDB data up to $p = 10$ as shown in Fig. 15.

Given Z_3 , Z_p can be modeled in the dissipation range by eq. (6.1). Fig. 16 shows ζ_{15} is not linear in $\ln(l/\eta)$ in the dissipation range. This is typical for $p > 10$, and we do not

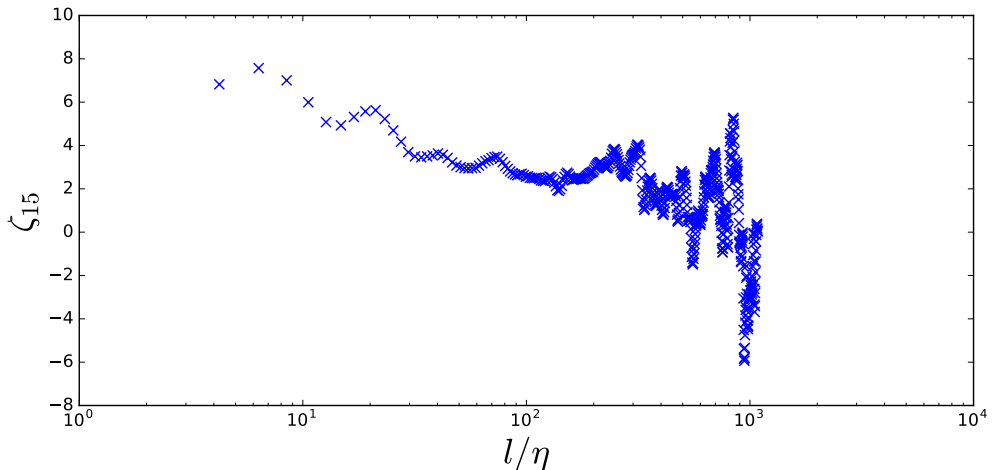


Figure 16: ζ_p is no longer linear in the dissipative range for $p > 10$.

include a model for ζ_p for larger p . The mismatch between the data and model for larger p raises the question whether the model needs to be improved, the numerical methods are unstable for high moments, or the data need improvement.

6.2. Full ζ_p parameterization

We have developed a model that captures the longitudinal velocity increments for all of the small length scales up to and including the inertial range. The ζ_p parameterization starts with $\zeta_p = a_p$ at the Kolmogorov length scale ($l/\eta = 1$) as shown in eq. (3.2). Based on eq. (6.1), a model for ζ_p that captures the linear segment in the dissipative range for each p with input Z_3 and a_3 value dependence is defined as:

$$\begin{aligned} \zeta_p^{dr} &= Z_p \cdot \ln\left(\frac{l}{\eta}\right) + a_p \\ &= \left(p/9 + 1 - (1/3)^{\frac{p}{3}}\right) \cdot \left(Z_3 \cdot \ln\left(\frac{l}{\eta}\right) + a_3\right). \end{aligned} \quad (6.3)$$

We have parameterized ζ_p for longitudinal velocity increments $\langle |\delta_l u|^p \rangle$ at the dissipation range with a finite number of parameters for p up to 10. It is p dependent, with the variables Z_3 and a_3 calculated from ζ_3 .

The dissipation range begins at the Kolmogorov length scale and ends at the intersection with the theoretical value from SL, which marks the start of the inertial range. This transition occurs approximately at the Taylor micro scale. The transition point can be found by

$$\left(p/9 + 1 - (1/3)^{\frac{p}{3}}\right) \cdot \left(Z_3 \cdot \ln\left(\frac{l}{\eta}\right) + a_3\right) = \zeta_p^{dr} = \zeta_p^{SL} = p/9 + 2 \cdot \left[1 - (2/3)^{\frac{p}{3}}\right]. \quad (6.4)$$

We solve this equation for length scale l with the known variable Z_3 and a_3 from ζ_3 data along with the known η . The p dependent transition points of ζ_p for $p = 2, 3, 6$ are shown as the thick plus symbols in Fig. 13.

7. The SL conjecture for the laminar limit

SL discusses the large p asymptotes of ϵ_l^p in developing parameters for their τ_p inertial range methodology. They predicted dominance by vortices in this regime. We come to the same conclusion in the large p asymptotes more directly through an analysis of ζ_p , which reflects the intensity of the vortical structures. We find in Fig. 14 and eq. (6.3) that ζ_p is increasing in p as the length l/η moves toward the dissipation range.

We interpret the length scale l/η limit in terms of Taylor-Green vortices continued past the instability point. Assuming the CC model remains applicable in this range, Fig. 12 analyzes the CC_∞ model and shows a nonzero residual value for T_2 and similarly for all T_p . Line vortices do not dissipate energy and are described by the vanishing τ_p for all p . The presence of non-zero T_p for all p indicates that the line vortices occur in an unstable state, as occurs in a Taylor-Green vortex, continued past its singular value.

8. Conclusions

We have extended scaling laws for longitudinal velocity increments and energy dissipation rate structure functions from the inertial range to all length scales by modifying their exponential scaling exponents. We verify the complete parameterization models for τ_p and ζ_p in the dissipation range, i.e. from the Kolmogorov scale to the Taylor scale, limited to $p \leq 10$ for ζ_p . Our major model feature, linearity of the log scale dissipation processes, is verified through comparison to the JHTDB and UMA data.

In local regions, even within a fully developed turbulent flow, the turbulence is not isotropic nor scale invariant due to the influence of larger turbulent structures (or their absence). For this reason, turbulence that is not fully developed is an important issue which the present analysis addresses.

In Kolmogorov theory and in advanced multifractal scaling law theories, ζ_2 has a range in which it is a flat line of constant value in log length scale, as observed. It has been noted that τ_p is not constant in the inertial range that is defined by ζ_2 . Our data analysis and data of others show no clearly defined inertial range for the energy dissipation rate. The τ_p peak is p dependent, but occurs approximately at the Taylor micro-scale. The transition from the dissipation range to the inertial range takes place near the Taylor micro-scale.

We find that the Chen and Cao model for τ_p can be extended across all length scales for small p moments. Our refined CC_q model describes the relation between any τ_p and τ_q exponents. The CC_∞ model complements the SL analysis of vortices in the $l/\eta \rightarrow 1$ limit are given.

9. Declaration of Interests

The authors report no conflict of interest.

REFERENCES

- ALMALKIE, S. & DE BRUYN KOPS, S. 2012 Energy dissipation rate surrogates in incompressible navierstokes turbulence. *Journal of Fluid Mechanics* .
- BOLDYREV, STANISLAV, NORDLUND, AKE & PADOAN, PAOLO 2002 Scaling relations of supersonic turbulence in star-forming molecular clouds. *The Astrophysical Journal* **573** (2), 678–684.
- CAO, NIANZHENG, CHEN, SHIYI & SHE, ZHEN-SU 1996 Scalings and relative scalings in the Navier-Stokes turbulence. *Phys. Rev. Lett.* **76**, 3711–3714.

- CHAVARRIA, GERARDO, BAUDET, CHRISTOPHE, BENZI, R. & CILIBERTO, SERGIO 1995*a* Hierarchy of the velocity structure functions in fully developed turbulence **5**.
- CHAVARRIA, GERARDO, BAUDET, CHRISTOPHE, BENZI, R. & CILIBERTO, SERGIO 1996 Scaling laws and dissipation scale of a passive scalar in fully developed turbulence. *Physica D: Nonlinear Phenomena* **99** (2), 369 – 380.
- CHAVARRIA, G. RUIZ, BAUDET, C. & CILIBERTO, S. 1995*b* Hierarchy of the energy dissipation moments in fully developed turbulence. *Phys. Rev. Lett.* **74**, 1986–1989.
- CHEN, SHIYI & CAO, NIANZHENG 1995 Inertial range scaling in turbulence. *Phys. Rev. E* **72**:R5757–R5759.
- FRICK, P., DUBRULLE, B. & BABIANO, A. 1995 Scaling properties of a class of shell models. *Phys. Rev. E* **51**, 5582–5593.
- FRISCH, U. 1996 *Turbulence: The Legacy of A. N. Kolmogorov*. Cambridge: Cambridge University Press.
- HE, GUOWEI, DOOLEN, GARY D. & CHEN, SHIYI 1999 Calculations of longitudinal and transverse velocity structure functions using a vortex model of isotropic turbulence. *Physics of Fluids* **11** (12), 3743–3748.
- KOLMOGOROV, A. N. 1941 Local structure of turbulence in incompressible viscous fluid for very large Reynolds number. *Doklady Akad. Nauk. SSSR* **30**, 299–3031.
- KOLMOGOROV, A. N. 1962 A refinement of previous hypotheses concerning the local structure of turbulence in a viscous incompressible fluid at high reynolds number. *J. Fluid Mechanics* **13**, 82–85.
- L. MILLER, PAUL & E. DIMOTAKIS, PAUL 1991 Stochastic geometric properties of scalar interfaces in turbulent jets. *Physics of Fluids A Fluid Dynamics* .
- LI, Y., PERLMAN, E., WAN, M., YANG, Y., BURNS, R., MENEVEAU, C., BURNS, R., CHEN, S., SZALAY, A. & EYINK, G. 2008 A public turbulence database cluster and applications to study Lagrangian evolution of velocity increments in turbulence. *Journal of Turbulence* **9** (31).
- MÜLLER, WOLF-CHRISTIAN & BISKAMP, DIETER 2000 Scaling properties of three-dimensional magnetohydrodynamic turbulence. *Phys. Rev. Lett.* **84**, 475–478.
- NOVIKOV, E. A. 1994 Infinitely divisible distributions in turbulence. *Phys. Rev. E* **50**, R3303–R3305.
- PERLMAN, E., BURNS, R., LI, Y. & MENEVEAU, C. 2007 Data Exploration of Turbulence Simulations using a Database Cluster. In *SC '07 Proceedings of the 2007 ACM/IEEE conference on Supercomputing*.
- SHE, Z. S. & LEVEQUE, E. 1994 Universal scaling laws in fully developed turbulence. *Phys. Rev. Lett.* **72**, 336–339.
- ZOU, ZHENGPING, ZHU, YUANJIE, ZHOU, MINGDE & SHE, ZHEN-SU 2003 Hierarchical structures in a turbulent pipe flow. *Fluid Dynamics Research* **33** (5), 493 – 508.